Supporting Information

English et al.

SI Materials and Methods

Sample preparation for mEos2 tracking. *E. coli* cells (MG1655) expressing the monomeric fluorescent protein mEos2 (1) from a plasmid derived from the pDendra2-B vector (Evrogen) are imaged on a M9-glucose agarose pad in a FCS2 flow chamber (Bioptechs). The MG1655 cells are grown overnight and diluted a thousand fold in M9 buffer containing amino acids (RPMI-1640, Sigma-Aldrich). The cells are then grown to an optical density at 600 nm of 0.05 and placed on an agarose pad (SeaPlaque GTG Agarose, Lonza) containing the same M9 medium. We observe leakage expression of mEos2 in the absence of inducer, and red mEos2 molecules are generated by the photoconversion laser beam at 405 nm.

Sample preparation for ribosomal time-lapse imaging. Using the genome integration approach based on site-specific recombination (2), we have C-terminally labeled three ribosomal proteins in three separate strains with Dendra2: S2, L19 and L31 . The advantage of this integration method is that it uniformly tags all the cellular ribosomes. This uniformity was confirmed by fluorescence flow cytometry (FCM) (Fig. S9*A*). S2, L19 and L31 were selected as suitable fusion targets since all three ribosomal proteins have solvent accessible C-termini.

E. coli cells (BW25993) expressing either S2-G-Dendra2, L19-G-Dendra2 or L31-G-Dendra2 from their native loci are imaged on a M9-glucose agarose pad in a FCS2 flow chamber (Bioptechs). The cells are grown overnight and diluted a thousand fold in M9 buffer containing amino acids (M5550, Sigma-Aldrich). The cells are then grown to an optical density at 600 nm of 0.05 and placed on an agarose pad (SeaPlaque GTG Agarose, Lonza) containing the same M9 medium. The temperature is held constant at 30 °C with an electrical cell heater and an objective heater (both Bioptechs). Both differential interference contrast and fluorescence snapshots are recorded every 5 min for 4 h as the cells are dividing on the agarose pad.

Sample preparation for RelA tracking. Using the genome integration approach based on site-specific recombination (2), we have C-terminally labeled RelA with Dendra2 using a glycine linker. This construct was selected for having the fastest growth recovery in ensemble Bioscreen experiments using plasmid expressed RelA fusions in Δ*relA* knockout strains (see Fig. S4), and growth curves of chromosomal fusions are compared in Fig. S6. The C-terminal RelA-Dendra2 fusion is full-length even when overexpressed (see Fig. S8). The advantage of this integration method is that it uniformly tags all the cellular RelA. Individual RelA trajectories are recorded via native chromosomal expression of a C-terminal chromosomal Dendra2-G-RelA fusion.

The cells are grown overnight and diluted a thousand fold in M9 buffer containing amino acids (M5550, Sigma-Aldrich). The cells are grown to an optical density at 600 nm of 0.05 and placed on an agarose pad (SeaPlaque GTG Agarose, Lonza) containing the same M9 medium. The temperature is held constant at 30 °C until the individual cells have formed small microcolonies on the agarose pad. Individual RelA trajectories are recorded after red Dendra2 is generated using short pulses of the photoconversion laser beam. The number of chromosomally expressed RelA-Dendra2 molecules per cell that can be photoconverted is often very low or sometimes zero, presumably due to a combination of limited maturation of Dendra2 and a low copy number of RelA molecules. To obtain adequate statistics we calculate CDFs and MSDs form all obtained

single-molecule RelA trajectories from the entire microcolony for each of the experimental conditions and for each frame-time.

For SHX experiments, the agarose pad is pre-soaked with a high concentration of L-SHX to a final concentration of 2.5 mM L-SHX. All *E. coli* cells (BW25993) expressing RelA-Glycine-Dendra2 from its native locus are imaged in a FCS2 flow chamber (Bioptechs). The temperature is held constant at 30 °C with an electrical cell heater and an objective heater (both Bioptechs).

For temperature upshift experiments the temperature is adjusted with the electrical heater elements. The temperature of the pad is recorded during the temperature upshift with a digital temperature sensor on the electrical enclosure.

Bulk growth recovery measurements for RelA constructs. We have selected our RelA-Dendra2 fusion in three steps.

First, we tested the functionality of the plasmid-expressed N-terminal Dendra2 fusion to RelA. We validated the functionality of this construct in a Δ*relA* background in a set of growth experiments in different media, testing it in two ways (Fig. S4). We tested it for dominant inhibitory effect in amino acid rich conditions, comparing the Δ*relA* strain with the same strain transformed with the plasmid expressing the fluorescent RelA derivative in question. We established that the construct had no significant deleterious effect on the bacterial growth (Fig. S4). Under conditions of amino acid starvation, either induced by concomitant removal of all amino acids and an overload of methionine and tryptophan (in-house modification of the valine overload approach (3)) (Fig. S4*A*) or by SHX (4) (Fig. S4*B* and Fig. S4*C*) the N-terminal RelA fusion proved to be functional as is evident from considerably earlier growth resumption (lower recovery time) as compared to the Δ*relA* strain.

Second, we compared the plasmid-encoded N- and C-terminal fusions of RelA under stringent conditions induced by concomitant removal of all amino acids and an overload of methionine and tryptophan (Fig. S5). The C-terminal fusion is more active in cellular growth recovery under the stringent conditions described above, and thus we choose this position for the Dendra2 fluorophore.

Finally, we varied the linker sequence of the C-terminal Dendra2 fusion construct integrated in the chromosome using the genome integration approach based on site-specific recombination (2). Two variants were constructed, dubbed as C-terminal Dendra2-1 and C-terminal Dendra2-2. Dendra2-1 has a glycine as a linker, whereas Dendra2-2 has a glycine-proline-glycine linker. These constructs were compared to the N-terminal chromosomally integrated Dendra2 fusion and to each other under stringent conditions either induced by concomitant removal of all amino acids and an overload of methionine and tryptophan (Fig. S6*A*) or by SHX (Fig. S6*B*). The C-terminal fusion C-terminal Dendra2-1's recovery from SHX induced starvation is 19 minutes faster than Dendra2-2, and is 3.5 hours faster as compared to the N-terminal chromosomal fusion strain. Dendra2-1 was selected and used for the SPT experiments throughout the paper.

See below for a detailed description of the Bioscreen growth assay, treatment of the growth curves and a list of used strains.

Protocol for the Bioscreen growth assay. Cells are grown overnight in buffer 1, re-diluted 500-fold in buffer 1 to an optical density at 600 nm of 0.05. Cells are diluted 50-fold into sterile 100-well honeycomb plates with covers (Bioscreen) containing buffer 1, 2, 3, 4 or 5. The optical density at 600 nm is measured using a Labsystems Bioscreen C

plate reader. Growth curves are measured at 37 °C after 5 min of pre-heating. Time points are recorded every 5 min after 30 s of shaking time with medium shaking intensity.

The starvation recovery growth curves are fit to:

$$\mathrm{OD}_{600}(t) = \begin{cases} max_{\mathrm{OD}} \Big/ \left(1 + \exp \dfrac{t_{\mathrm{half\ OD}}}{rate}\right), & t < t_{\mathrm{delay}} \\ max_{\mathrm{OD}} \Big/ \left(1 + \exp \dfrac{t_{\mathrm{half\ OD}} - (t - t_{delay})}{rate}\right), & t \geq t_{\mathrm{delay}} \end{cases}$$

From the fit we obtain the recovery time t_{delay}, which we mark in Figs. S4 to S6.

Bioscreen buffers

Buffer 1 (M9 + AA): **MEM Amino Acids (M5550, Sigma-Aldrich)**, M9 salts, 2 mM $MgSO_4$, 0.1 mM $CaCl_2$, 0.4 % (w/v) glucose, MEM Vitamins (M6895, Sigma-Aldrich), (and 89 μM Uracil (10 μg/mL) for MG1655 (Δ*relA*) strains).
Buffer 2 (M9): M9 salts, 2 mM $MgSO_4$, 0.1 mM $CaCl_2$, 0.4 % (w/v) Glucose, MEM Vitamins (M6895, Sigma-Aldrich), (and 89 μM Uracil (10 μg/mL) for MG1655 (Δ*relA*) strains).
Buffer 3 (M9 + Met + Trp): **6.5 mM methionine (1g/ L), 4.7 mM tryptophan (1 g/L)**, M9 salts, 2 mM $MgSO_4$, 0.1 mM $CaCl_2$, 0.4 % (w/v) Glucose, MEM Vitamins (M6895, Sigma-Aldrich), (and 89 μM Uracil (10 μg/mL) for MG1655 (Δ*relA*) strains).
Buffer 4 (M9 + AA + 2.5 mM SHX): **2.5 mM L-Serine Hydroxamate**, MEM Amino Acids (M5550, Sigma-Aldrich), M9 salts, 2 mM $MgSO_4$, 0.1 mM $CaCl_2$, 0.4 % (w/v) glucose, MEM Vitamins (M6895, Sigma-Aldrich), (and 89 μM Uracil (10 μg/mL) for MG1655 (Δ*relA*) strains).
Buffer 5 (M9 + AA + 0.5 mM SHX): **0.5 mM L-Serine Hydroxamate**, MEM Amino Acids (M5550, Sigma-Aldrich), M9 salts, 2 mM $MgSO_4$, 0.1 mM $CaCl_2$, 0.4 % (w/v) glucose, MEM Vitamins (M6895, Sigma-Aldrich), (and 89 μM Uracil (10 μg/mL) for MG1655 (Δ*relA*) strains).

Strains analyzed in the Bioscreen growth assay

1: MG1655(Δ*relA*) (kindly provided by Dr. Santanu Dasgupta).
2: MG1655(Δ*relA*) + plasmid 10 (Dendra2–Glycine–RelA, Evrogen pDendra2-B plasmid backbone).
3: MG1655(Δ*relA*) + plasmid 1-1 (Dendra2–Glycine–RelA, pET24 plasmid backbone).
4: MG1655(Δ*relA*) + plasmid I1 (RelA–Glycine–Dendra2, pET24 plasmid backbone).
5: BW25993 (kindly provided by Dr. Paul Choi).
6: BW25993 with C–terminal chromosomal insertion (RelA–Glycine–Dendra2) (dubbed C-terminal Dendra2-1).
7: BW25993 with C–terminal chromosomal insertion (RelA–Glycine–Proline–Glycine–Dendra2) (dubbed C-terminal Dendra2-2).
8: BW25993 with N–terminal chromosomal insertion (Dendra2-RelA) (dubbed N-terminal Dendra2-1).

SMG test for relaxed phenotype

A classical test for relaxed phenotype is the so-called “serine, methionine, glycine” (SMG) plate test (5) which selectively inhibits growth of the relaxed K12-based *E. coli* strains. We

use a more selective version of the SMG plate test, where SMG is supplemented with 100 µg/ml leucine (M. Cashel, personal communication). We scored plates after 48 h of incubation at 37 °C. As evident from Fig. S7, RelA-Dendra2 rescues the relaxed phenotype and supports growth on the SMG plates.

Optimization of the stroboscopic imaging conditions for mEos2 tracking. The duration of the excitation pulse is a critical parameter for obtaining distinct fluorescence spots from the rapidly moving single molecules. The optimal value is a tradeoff between collecting the large numbers of photons needed to determine the position of the molecule accurately and minimizing the broadening of the spot due to diffusion of the molecule during the excitation pulse. While we could easily freeze any movement within a diffraction-limited spot using pulses shorter than 200 µs, the fitting precision is proportional to the square root of the number of detected photons (6) and precise localization is not possible given the poor photo-physical properties of mEos2 and hence we image at higher illumination pulse durations.

The photoconversion approach is much more controllable than fine-tuning of GFP induction, which is non-linear in inducer concentration (7). We can fine-tune the number of red mEos2 molecules by modulating either the photoconversion laser intensity or pulse-length. This can be done at much higher time resolution (milliseconds vs. typically several hours due to slow maturation rates of current dyes) and photoconversion pulses can be applied multiple times during the same experiment.

The photoconversion frequency and laser power are adjusted for each cell to have on average less than one fluorophore visible at any given time.

Characterization of the apparent diffusion coefficients of mEos2. Single-molecule tracking of small protein molecules has scientific value *per se*: the nature of how they diffuse in the crowded bacterial cytosol is a matter of debate for decades already, and it is commonly assumed that the intracellular diffusion is anomalous (8, 9). Sub-diffusion, where $<\Delta x(t)^2> \propto t^{\alpha}$ with $\alpha < 1$, has been observed for large complexes in the bacterial cytoplasm (10) as well as for molecules in cell membranes (11). If the movement of individual protein molecules in the cytoplasm were also sub-diffusive it would profoundly affect the validity of test-tube experiments as *in vivo* models.

The single-molecule diffusion trajectories are analyzed by calculating MSDs (12, 13) for all possible time intervals in the sample (*x*-*y*) plane and along the long axes of the cells (see Fig. 2D and Fig. S1). For all eight cells, cell-averaged apparent diffusion coefficients of $9.0 \pm 0.8\ \mu m^2\ s^{-1}$ (sample plane) is obtained from the MSDs over 4 ms (see Table S1). From the slopes of the MSDs from 4 to 8 ms, we obtain cell-averaged apparent diffusion coefficients of $4.1 \pm 0.8\ \mu m^2\ s^{-1}$(in the sample plane). A strong correlation between apparent diffusion coefficients and cell sizes indicates that these coefficients are not microscopic diffusion coefficients (see Table S3).

Quantitative characterization of the *microscopic* diffusion behavior of mEos2. In Fig. S1 we show experimental MSD curves calculated along the long axis obtained from 8 individual *E. coli* cells. The curves cannot be directly compared since the MSDs plateau at different levels due to the different cell geometries of the eight cells. Instead, we compare the experimental data points to MSD curves calculated from simulated normal diffusion trajectories within the respective cell geometries. The microscopic diffusion coefficients obtained from the best fit of simulations to each experimental MSD curves are in the range of 11.5 to 13.5 $\mu m^2\ s^{-1}$. The good fits suggest that cytoplasmic diffusion

in all eight cells is indistinguishable from a Brownian walk, at least down to 4 ms (see Table S2).

The next question is whether or not the 0.6 $\mu m^2 s^{-1}$ spread in the observed microscopic diffusion coefficients is due to actual cell-to-cell variability. We test if one microscopic diffusion coefficient of 13 $\mu m^2 s^{-1}$ can adequately describe all of our data obtained from all eight cells. As can be seen in Fig. S1**,** all eight experimental MSD curves fall within their respective confidence intervals. The intervals are obtained from simulations with the same finite number of trajectories as in the corresponding experiments, and with a diffusion coefficient of 13 $\mu m^2 s^{-1}$. This implies that the small mEos2 protein may indeed perform simple Brownian motion at the same rate in all cells.

Microscopic diffusion simulations. The simulations consist of 3D random walks sampled at the 10 μs timescale in cells with experimentally obtained geometries. The starting points of the trajectories are sampled from a uniform distribution. The trajectory lifetimes are determined probabilistically to correct for uneven illumination such that the spatial distribution of simulated molecules is equal to that of experimental data. Each trajectory is terminated such that the average number of points in a trajectory is approximately equal for experimental and simulated trajectories.

We add two types of noise to the simulated trajectories. We first sample movement noise from a normal distribution. This accounts for the uncertainty in the position of the molecule, which arises from the movement of the molecule during the exposure time. We then add normally distributed fitting noise, which arises from the limited number of photons that are detected from the molecule during the exposure time.

The microscopic diffusion coefficients are determined by fitting the whole MSD curves to simulated data considering the geometry of the cells (see Fig. S1). The excellent agreement with a normal diffusion model for our experimental timescale does not rule out faster diffusion at timescales faster than 4 ms. Faster diffusion behavior of mEos2 at the sub-millisecond timescale may be contributing to experimental noise at 4 ms and longer timescales, which would manifest itself in a small offset in our experimental MSD curves.

We test the hypothesis that the microscopic diffusion coefficient is the same for all cells. For each cell, we overlay 99% confidence intervals on top of the experimental MSD curve. The 99% confidence intervals are calculated from simulated trajectories given the cell-specific geometry, the same number of trajectories and a universal diffusion coefficient of $13\,\mu m^2\ s^{-1}$. When we correct for multiple testing, the 99% confidence level for each individual test corresponds to a 95% confidence level for all cells. Since the MSD curves fall within their respective confidence interval we cannot reject the hypothesis that the diffusion coefficient actually is the same in all cells.

Ensemble photoactivation experiment. We can convert the photoconversion laser from wide-field excitation to confocal excitation mode via a flip-lens (see Fig. 1*B*). This allows us to record ensemble photoactivation (PA) data to complement our single-molecule analysis for the same individual *E. coli* cells (see Fig. S2).

To obtain the diffusion coefficient from the ensemble photoactivation experiment we fit a theoretical normal diffusion model to the experimental intensities. The experimental intensities are first averaged over four consecutive photoactivation time series of 30 frames taken over 120 ms. The preactivation background fluorescence is subtracted from each frame and the experimental intensities are projected on the long axis (*x*-axis)

of the cell (length L), resulting in the experimental intensity distribution $F_{\mathrm{exp}}(x,t)$. The fluorescence intensity is modeled by the one-dimensional diffusion equation $\partial F_{\mathrm{mod}}(x,t)/\partial t = D\,\partial^2 F_{\mathrm{mod}}(x,t)/\partial x^2$ with reflecting boundaries. The equation is integrated from the initial condition given by the fluorescence intensity distribution in the first camera frame after photoactivation. The diffusion coefficient is optimized such that the model error $\int_{x=0.2\,L}^{0.8\,L}\int_{t=0\,ms}^{120\,ms}\left(F_{\mathrm{exp}}(x,t)-\alpha(t)\,F_{\mathrm{mod}}(x,t)\right)^2$ is minimized. Photobleaching in the experimental data is corrected for by the factor $\alpha(t)=\int_x F_{\mathrm{exp}}(x,t)\,/\int_x F_{\mathrm{exp}}(x,0)$. The error norm is only minimized over the central part of the cell, $x\in[0.2\,L, 0.8\,L]$, since the polar regions have a disproportionally small intensity when projected to one dimension.

When we use PA to determine the diffusion coefficient of mEos2 under our experimental conditions, our best estimate is $11\,\mu m^2\,s^{-1}$. This value is in reasonable agreement with our single-molecule experiment. However, this ensemble estimate is very dependent on the assumed geometry of the individual cell as was noted already by Elowitz *et al.* (14).

SI Tables

Table S1. Apparent diffusion coefficients $\left(D_{x-y}\right)$ in the sample (*x*-*y*) planes of eight *E. coli* cells. The apparent diffusion coefficients are calculated from mean square displacements (MSDs) over 4 ms and the slopes of the MSDs from 4 to 8 ms.

Cell number	Exposure Time (ms)	Frame time (ms)	Cell length $(\mu\mathrm{m})$	Apparent D_{x-y} (MSD, 4 ms) $\left(\mu\mathrm{m}^2\ \mathrm{s}^{-1}\right)$	Apparent D_{x-y} (MSD, 4 to 8 ms) $\left(\mu\mathrm{m}^2\ \mathrm{s}^{-1}\right)$
1	1	4	3.0	10.4	5.1
2	1	4	2.1	9.0	3.5
3	1	4	2.1	9.1	3.6
4	1	4	2.0	8.2	4.0
5	1	4	2.3	8.2	4.6
6	1	4	2.0	8.2	3.6
7	1	4	1.8	8.8	3.1
8	1	4	2.5	10.0	5.3
Average			2.2	9.0	4.1
Standard deviation			0.4	0.8	0.8

Table S2. Microscopic diffusion coefficients (D_{micro}). The microscopic diffusion coefficients are obtained by simulating trajectories assuming normal diffusion in the volumes defined by the geometries of the cells. The diffusion coefficients are iteratively adjusted to find the best possible match between experimental mean square displacements (MSDs) and average MSDs obtained from many simulations (see Fig. S1).

Cell Number	Exposure time (ms)	Frame time (ms)	Cell length (μm)	D_{micro} ($\mu m^2\ s^{-1}$)
1	1	4	3.0	**12.5**
2	1	4	2.1	**11.5**
3	1	4	2.1	**13**
4	1	4	2.0	**13**
5	1	4	2.3	**12.5**
6	1	4	2.0	**12**
7	1	4	1.8	**13**
8	1	4	2.5	**13.5**
Average			2.2	**12.6**
Standard deviation			0.4	**0.6**

Table S3. Pearson's correlation coefficients of diffusion coefficients and cell lengths. The correlation coefficient for the microscopic diffusion coefficients (D_{micro}) is in bold. While D_{micro} display no correlation, the apparent diffusion coefficients along the long axes (D_x) and in the sample (*x*-*y*) planes (D_{x-y}) of eight *E. coli* cells are strongly correlated to the cell lengths.

	$\boldsymbol{D_{micro}}$	Apparent D_x	Apparent D_{x-y}	Apparent D_x	Apparent D_{x-y}
		(MSD, 4 ms)	(MSD, 4 ms)	(MSD, 4 to 8 ms)	(MSD, 4 to 8 ms)
Cell length	**0.07**	0.56	0.78	0.84	0.86

SI Figures

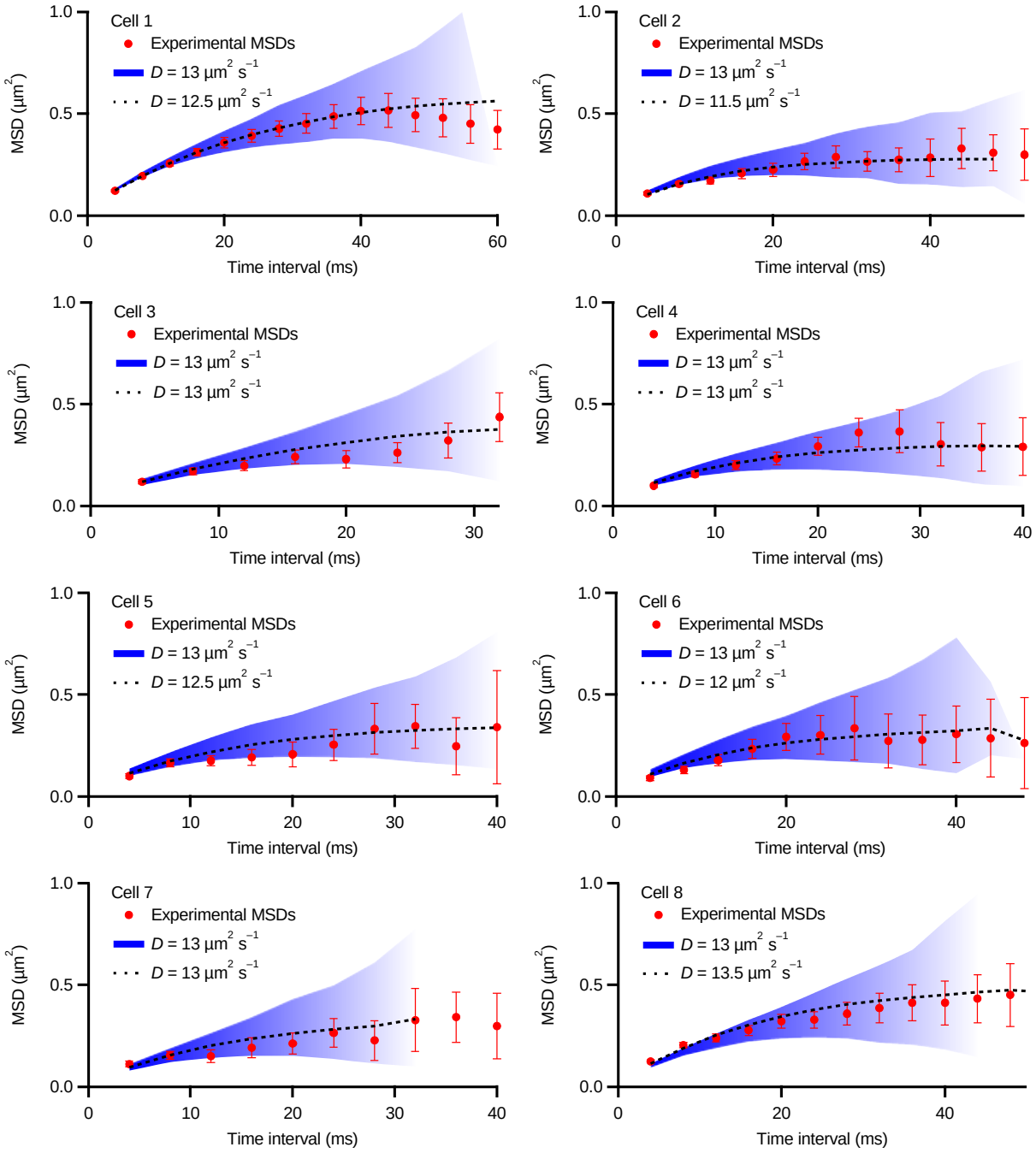

Fig. S1. Mean square displacements (MSDs) along the long axes of eight *E. coli* cells. Experimental MSDs and error bars representing experimental standard errors of the means are displayed in red. The confidence intervals (blue) are obtained from simulations in the volumes defined by the geometries of these cells by calculating and sorting MSDs for trajectories using a diffusion coefficient of 13 $\mu m^2 s^{-1}$. The average MSDs (black, dashed) are also obtained from simulations. Here we vary the diffusion coefficient for each cell to obtain the closest match to the experimental curve.

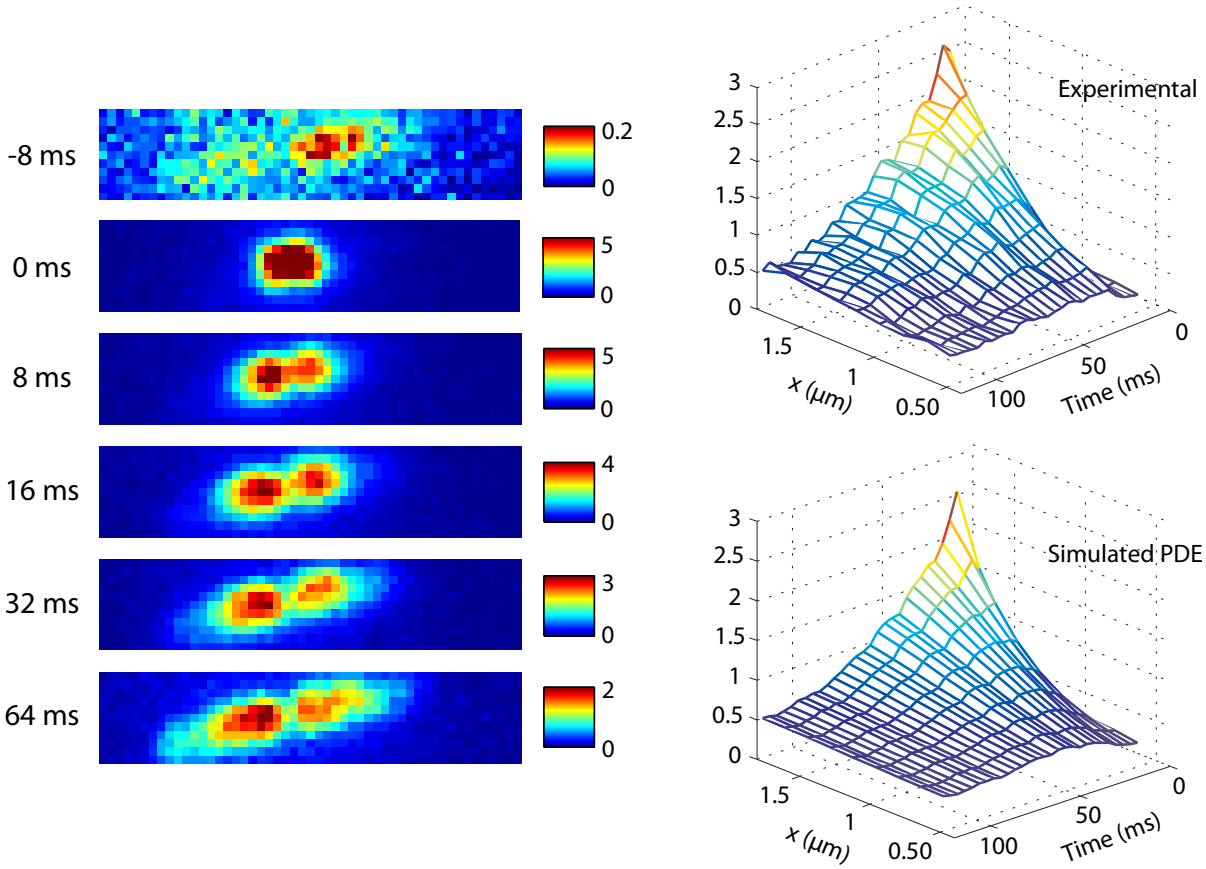

Fig. S2. Single cell photoactivation ensemble experiment. Left panel: A large number of mEos2 molecules are activated in a diffraction-limited region at the interface of two *E. coli* cells at time zero. mEos2 spreads throughout the two cells over a time period of 64 ms. Right top: The experimental fluorescence intensity values from the central part of the left cell (cell 5) are projected on the long (x) axis and plotted in the (x, t)-plane. Right below: Solution of the 1D diffusion equation time-evolved with reflective boundaries corresponding to the length of the cell. A diffusion coefficient of 11 μm^2 s^{-1} is obtained by fitting this solution to the experimental diffusion surface (right top).

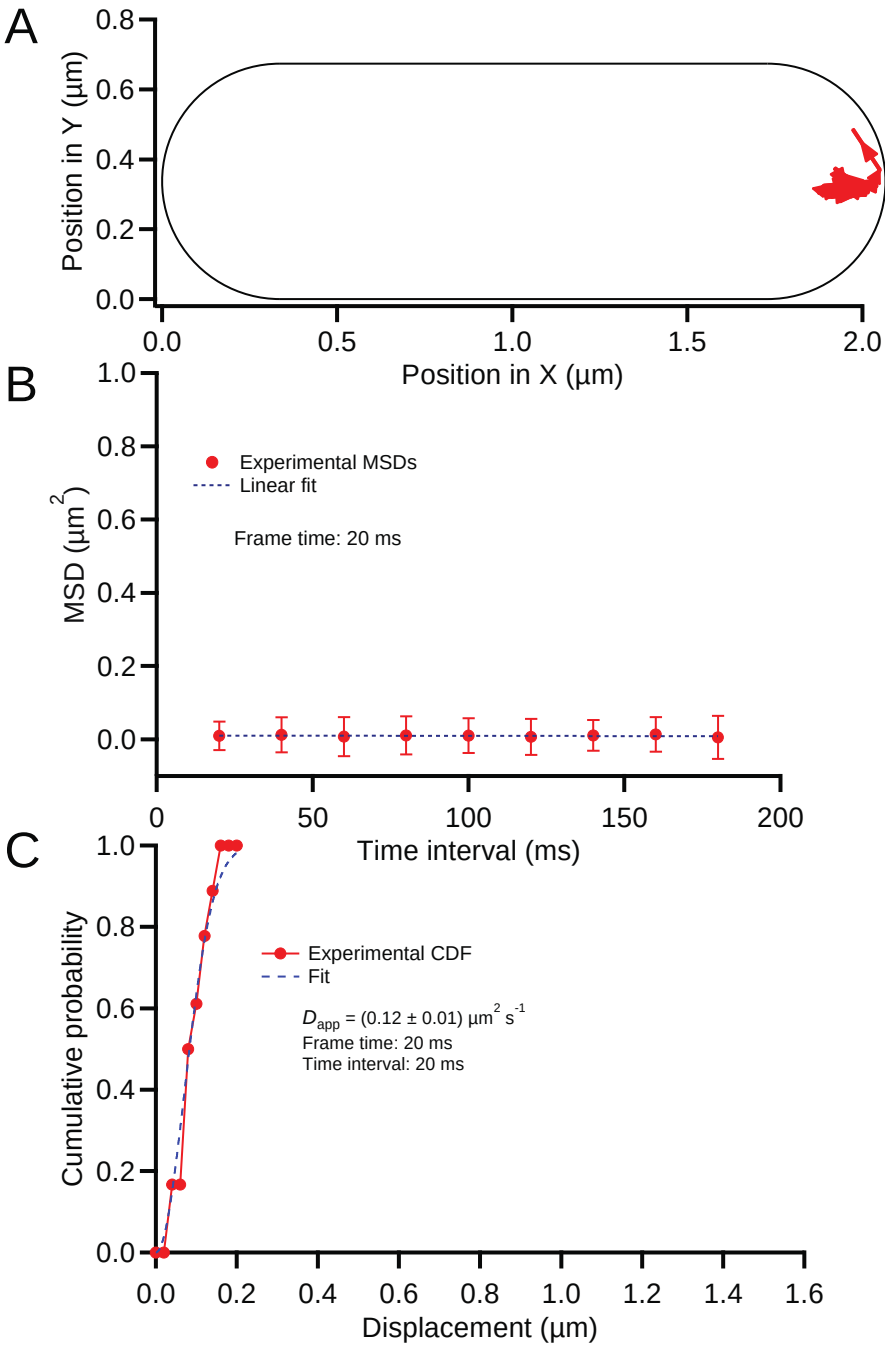

Fig. S3. Single molecule ribosome tracking of a stuck ribosome at the cell pole. (*A*) An experimentally obtained single molecule ribosome trajectory at the cell pole with a frame time of 20 ms and an exposure time of 0.8 ms. (*B*) Mean square displacements (MSDs) in the sample plane for this ribosomal trajectory at the pole. The MSD curve is flat. (*C*) Cumulative distribution function (CDF) of the displacements in the sample plane.

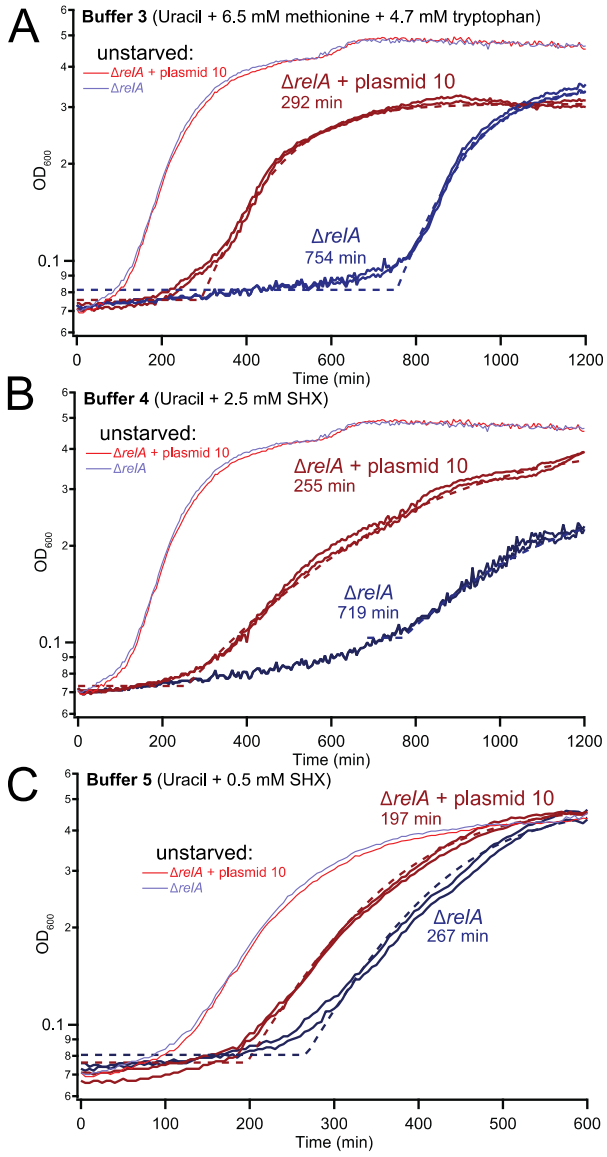

Fig. S4. Growth recovery by leakage expression of plasmid expressed N-terminal Dendra2 fusion to RelA. (*A*) Stringent response is induced by concomitant removal of all amino acids and an overload of methionine and tryptophan (buffer 3). The *E. coli* MG1655 *relA* deletion strain (Δ*relA*) recovers in 12.5 h (purple, duplicate runs). The same strain with leakage expression of Dendra2–Glycine–RelA from plasmid 10 speeds up the recovery by 7.7 h (brown, duplicate runs). Both unstarved curves are identical. (*B*) Stringent response induced by 2.5 mM of L–Serine Hydroxamate. The *relA* deletion strain recovers from this starvation in 12 h (purple, duplicate runs). Leakage expression of Dendra2–Glycine–RelA from plasmid 10 speeds up the recovery by 7.7 h (brown, duplicate runs). (*C*) Stringent response induced by 0.5 mM L–Serine Hydroxamate. The *relA* deletion strain recovers in 4.5 h (purple, duplicate runs). Leakage expression of Dendra2-Glycine-RelA speeds up this recovery by 1.2 h (brown, duplicate runs).

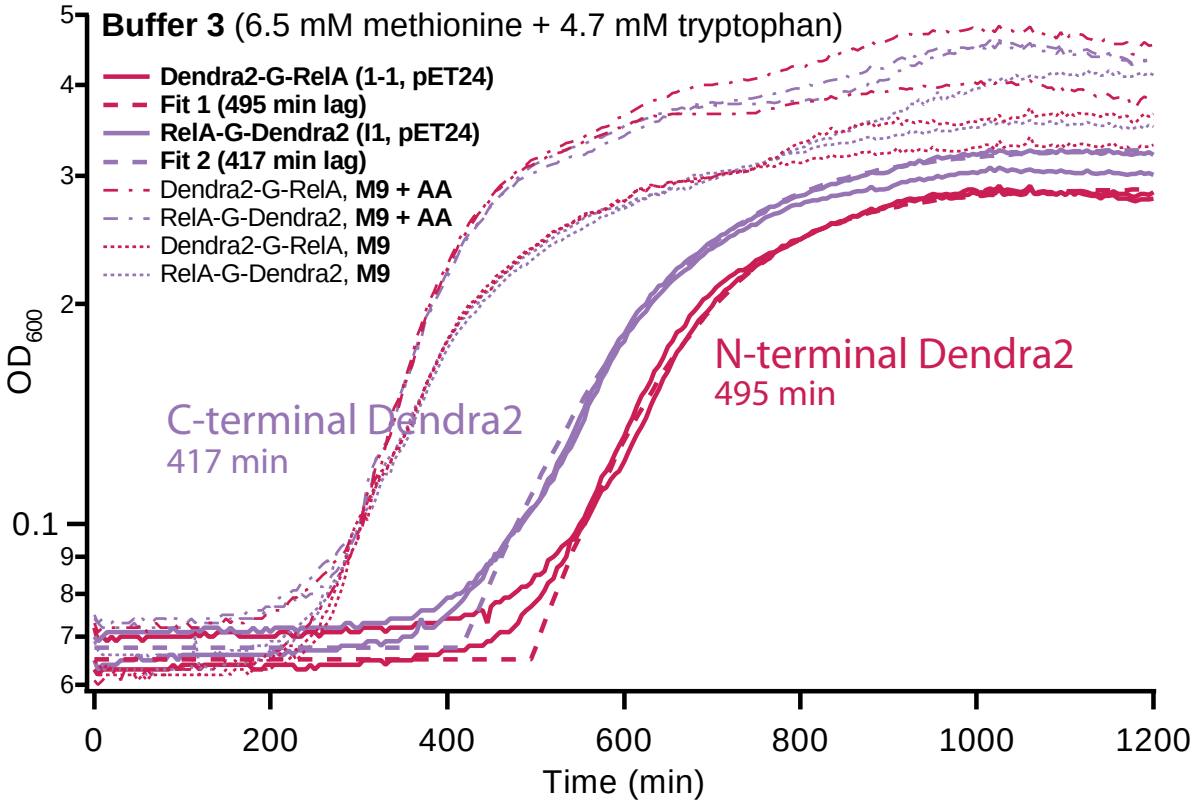

Fig. S5. Growth recovery comparison between C- and N-terminal Dendra2 fusions to RelA. Stringent response induced by concomitant removal of all amino acids and an overload of methionine and tryptophan. Leakage expression of RelA–Glycine–Dendra2 from plasmid I1 speeds up the recovery from starvation by 1.3 h (duplicate runs in purple) over N–terminally labeled RelA (Dendra2–Glycine–RelA from plasmid 1–1) (duplicate runs in crimson). When diluted in M9 + AA (buffer 1, dash-dotted curves) or in M9 buffer (buffer 2, dotted curves), the growth curves of Δ*relA* with and without any of the plasmids are almost identical.

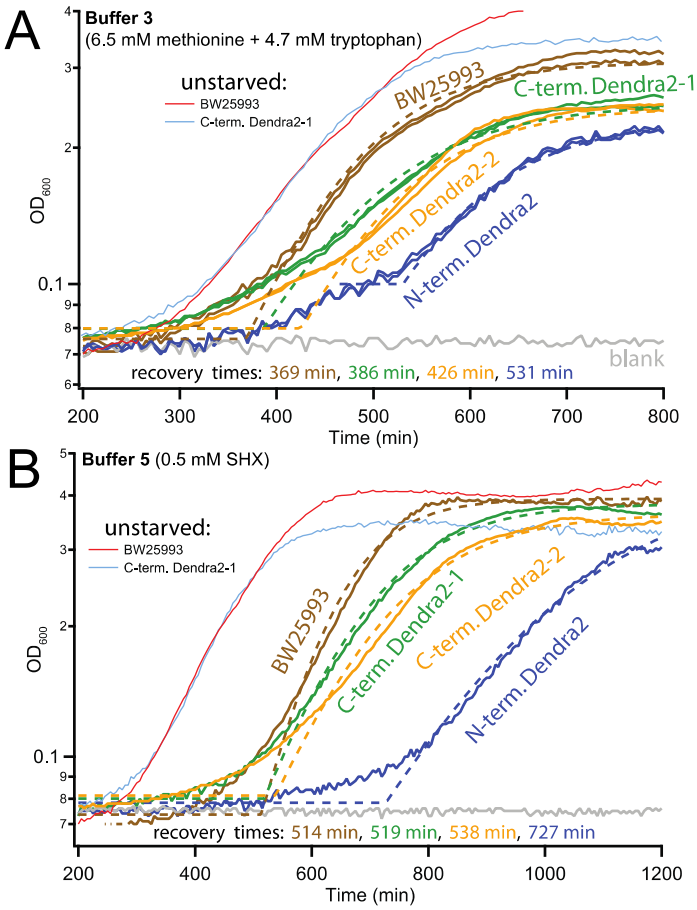

Fig. S6. Growth recovery comparison of chromosomal Dendra2 fusions to RelA. (*A*) Bulk growth recovery comparison of three chromosomal RelA-Dendra2 integrations. Stringent response is induced by concomitant removal of all amino acids and an overload of methionine and tryptophan. The three chromosomal fusions of Dendra2 to RelA in BW25993 all have different recovery times. As in Fig. S5, the C–terminal fusion outperforms the N–terminal fusion of Dendra2 to RelA. Duplicate growth curves of wild type BW25993 are depicted in brown. Duplicate runs of growth curves are displayed for C–terminal chromosomal Dendra2 integrations with a glycine linker (green) and with a Glycine–Proline–Glycine linker (yellow). Duplicate runs of the N–terminal fusion (Dendra2-RelA) are displayed in purple. When diluted in M9 + AA (buffer 1), the growth curves of BW25993 (red) and C-terminal Dendra2-1 (blue) are almost identical. (*B*) Bulk growth recovery comparison of three chromosomal Dendra2 RelA integrations. Stringent response is induced by 0.5 mM L–Serine Hydroxamate. The N–terminal Dendra2–RelA fusion (purple) recovers 3.6 h slower than wild type BW25993 (brown). The C–terminal RelA–Glycine–Proline–Glycine–Dendra2 fusion (yellow) recovers only 24 min slower than BW25993. The best chromosomal fusion has a glycine linker (RelA–Glycine–Dendra2, green), and recovers 3.5 h faster than our N–terminal chromosomal fusion of Dendra2 to RelA. When diluted in M9 + AA (buffer 1), the growth curves of BW25993 (red) and C-terminal Dendra2-1 (blue) are almost identical.

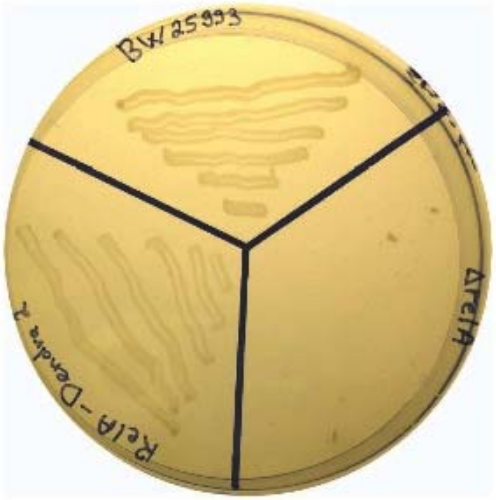

Fig. S7. Growth comparison on "serine, methionine, glycine" (SMG) plates. A classical test for relaxed phenotype is the so-called "serine, methionine, glycine" (SMG) plate test (5) which selectively inhibits growth of the relaxed K12-based *E. coli* strains. We use a more selective version of the SMG plate test, where SMG is supplemented with 100 µg/ml leucine. We scored plates after 48 h of incubation at 37 °C. RelA-Dendra2 rescues the relaxed phenotype and supports growth on the SMG plates.

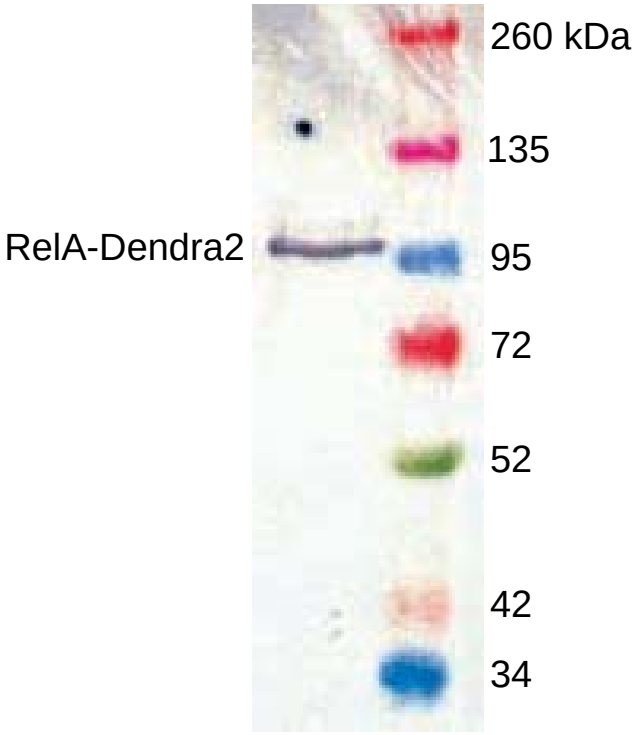

Fig. S8. Western blotting analysis. Western blot of plasmid-overexpressed C-terminal RelA-G-Dendra2 with anti-Dendra2 antibodies. The expected molecular weight for RelA-Dendra2 is 111 kDa.

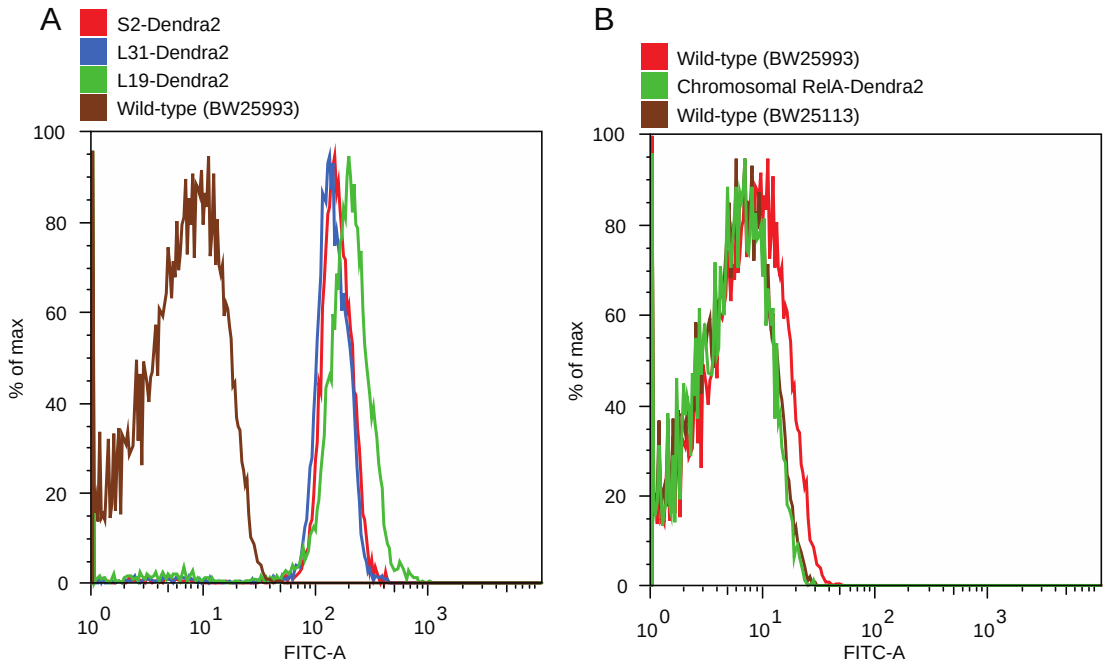

Fig. S9. Fluorescence Flow Cytometry (FCM) experiments. Stationary phase cultures were diluted 1:100 in fresh M9 medium and 30 µL samples were withdrawn, mixed with an equal volume of 30% glycerol in PBS and stored at −70 °C pending analysis on a flow cytometer (LSR II; BD Biosystems). The software packages BD FACSDiva and FlowJo were used to analyze the data. (*A*) FCM of S2, L19, L31 and wild-type BW25993 *E. coli* cells. The observed cellular uniformity in terms of fluorescence intensities suggests that a homogeneous cellular population was created. This underscores the advantage of the chromosomal integration method as it uniformly tags all the cellular ribosomes. (*B*) FCM of RelA-Dendra2, BW25113 and BW25993 *E. coli* cells. Low *in vivo* RelA concentrations render RelA-Dendra2 fluorescence undetectable by fluorescence flow cytometry. Two wild type *E. coli* strains (BW25113 and BW25993) were used to show that strain-specific variation in fluorescence is higher than the signal from RelA-Dendra2.

SI References

1. McKinney SA, Murphy CS, Hazelwood KL, Davidson MW, Looger LL (2009) A bright and photostable photoconvertible fluorescent protein. *Nat Methods* 6:131–133.
2. Datsenko KA, Wanner BL (2000) One-step inactivation of chromosomal genes in Escherichia coli K-12 using PCR products. *Proc Natl Acad Sci U S A* 97:6640-6645.
3. Leavitt RI, Umbarger HE (1962) Isoleucine and valine metabolism in Escherichia coli. XI. Valine inhibition of the growth of Escherichia coli strain K-12. *J Bacteriol* 83:624-630.
4. Tosa T, Pizer LI (1971) Biochemical bases for the antimetabolite action of L-serine hydroxamate. *J Bacteriol* 106:972-982.
5. Uzan M, Danchin A (1976) A rapid test for the rel A mutation in E. coli. *Biochem Biophys Res Commun* 69:751-758.
6. Thompson RE, Larson DR, Webb WW (2002) Precise nanometer localization analysis for individual fluorescent probes. *Biophys J* 82:2775–2783.
7. Choi PJ, Cai L, Frieda K, Xie S (2008) A stochastic single-molecule event triggers phenotype switching of a bacterial cell. *Science* 322:442-446.
8. Dix JA, Verkman AS (2008) Crowding effects on diffusion in solutions and cells. *Annu Rev Biophys* 37:247-263.
9. Magdziarz M, Weron A, Burnecki K, Klafter J (2009) Fractional brownian motion versus the continuous-time random walk: a simple test for subdiffusive dynamics. *Phys Rev Lett* 103:180602.
10. Golding I, Cox EC (2006) Physical nature of bacterial cytoplasm. *Phys Rev Lett* 96:098102.
11. Ghosh RN, Webb WW (1994) Automated detection and tracking of individual and clustered cell surface low density lipoprotein receptor molecules. *Biophys J* 66:1301-1318.
12. Deich J, Judd EM, McAdams HH, Moerner WE (2004) Visualization of the movement of single histidine kinase molecules in live *Caulobacter* cells. *Proc Natl Acad Sci USA* 101:15921–15926.
13. Niu L, Yu J (2008) Investigating intracellular dynamics of FtsZ cytoskeleton with photoactivation single-molecule tracking. *Biophys J* 95:2009–2016.
14. Elowitz MB, Surette MG, Wolf PE, Stock JB, Leibler S (1999) Protein mobility in the cytoplasm of Escherichia coli. *J Bacteriol* 181:197-203.